Effects of Cu and Mn dopings on the structural, optical, and magnetic properties of $Zn_{0.98}Fe_{0.02}O$ nanopowders

S. A. Ahmed[1,2,*]

[1] *Physics Department, Faculty of Science, Sohag University, Sohag 82524, Egypt*
[2] *Physics Department, College of Arts and Science, Qassim University, P.O. 3137, Unayzah 51911, Saudi Arabia*

ABSTRACT

This paper reports on the structural and magnetic properties of $Zn_{0.98-x}Fe_{0.02}(Cu/Mn)_xO$ ($x = 0.0$ and 0.02) nanopowders synthesized using a solid-state reaction method. Ultraviolet–Visible spectroscopy measurements demonstrated that the bandgap increased in the Fe-doped ZnO and decreased in both the Cu- and Mn-doped $Zn_{0.98}Fe_{0.02}O$. Photoluminescence studies confirmed the formation of oxygen vacancies (V_O) in all of the samples. The magnetization measurements revealed that the doping of Cu or Mn ions in $Zn_{0.98}Fe_{0.02}O$ increased the saturation magnetization (M_s). The M_s value of the Cu-doped $Zn_{0.98}Fe_{0.02}O$ is about five times larger than that of the undoped ZnO. The M_s value of the Mn-doped $Zn_{0.98}Fe_{0.02}O$ is of a magnitude larger than that obtained for the Cu-doped $Zn_{0.98}Fe_{0.02}O$, and it is about one and a half times larger than the magnitude of the $Zn_{0.98}Fe_{0.02}O$ and seven times larger than the magnitude of the undoped ZnO. We believe that the ferromagnetism is intrinsic, and it results from the interactions induced by the V_O incorporated into the ZnO lattice.

Introduction

Dilute magnetic semiconductors (DMSs) fabricated by doping transition metal (TM) ions into nonmagnetic semiconductors are receiving increasing attention due to their possible application in spin electronics [1]. Wide-gap DMSs combine their electrical conductivity with ferromagnetism (FM) and optical transparency, thus opening up the potential for their use in other devices. A wide-bandgap wurtzite-phase semiconductor ZnO ($E_g = 3.4$ eV) doped with TMs has been theoretically hypothesized as one of the most favorable types of DMS materials for room-temperature (RT)

applications [2]. FM above RT has previously been theoretically hypothesized [2–4], and it has been experimentally shown for TM dopants in bulk, powder, nanowire, and thin-film forms of ZnO [5–9]. Besides, many studies have revealed that the ferromagnetic properties of TM-doped metal oxides strongly depend on the metal–oxide host system, surface defects, particle size, and TM dopant type and concentration [5–11]. These studies, however, did not lead to consistent conclusions. There is no clear agreement about the nature and origin of the observed FM in the diluted magnetic oxide doped with a few percents of 3d cations. Therefore, more intensive and

Address correspondence to E-mail: saadzf2003@gmail.com

extensive work is essential as the mechanism in ZnO-based DMSs is still far from being well understood.

Among the TM ions, the incorporation of Fe^{2+} into the ZnO lattice promises to bring about very interesting and novel magnetic, electric, and optical properties. Moreover, Fe-doped ZnO nanostructures are very useful in a variety of applications such as gas sensors, solar cells, optoelectronic devices, and flat-panel displays [12]. The RT FM in Fe-doped ZnO is also still in debate. Sharma et al. [13] demonstrated that 1% Fe-doped ZnO samples show diamagnetic character, while ferromagnetic nature is observed for 2 and 3% Fe-doped samples, and higher doping of Fe, paramagnetic (PM) nature dominates. Han et al. [14] failed to obtain RT FM in Fe-doped ZnO bulk samples and suggested that the additional Cu doping is essential to achieve RT FM in these samples. Hence, although magnetism in Fe-doped ZnO nanoparticles is an interesting and controversial issue to be resolved, tailoring of their ferromagnetic behaviors by codoping has immense importance for device applications. So far, many experimental results about codoping have been reported, aimed at enhancing their magnetization. The codoping, i.e., the simultaneous presence of two kinds of TM dopant, has drawn attention mainly due to the possibility of using it to tailor the position and occupancy of the Fermi energy (E_F) of doped DMS. So, the codoping with another magnetic species is a possible approach for editing the ferromagnetic response of TM-doped ZnO [15].

Along the above line of approach, attempts have been made to fabricate ZnO-based DMS by codoping two TM elements: (Fe, Mn) or (Fe, Cu). $Zn_{0.8}Fe_{0.1}Mn_{0.1}O$ single crystalline nanoparticles (~ 7 nm) were synthesized using the low-temperature chemical "pyrophoric reaction process" [16]. The magnetization measurements demonstrated that the doping of Mn ions in ZnFeO nanomaterials decreases the coercive field and average magnetization values, which was attributed to the formation of antiferromagnetic or PM states in a ferromagnetic infinite cluster through the doping of Mn ions. Fan et al. also prepared (Mn, Fe)-codoped ZnO powders and thin films with a ferromagnetic property at RT, but their results showed that FM originated from the impurities of the magnetic clusters in the vacuum-annealed $Zn_{0.98}Mn_{0.01}Fe_{0.01}O$ powder at 600 °C, while the FM of (Mn, Fe)-codoped ZnO DMS films is an intrinsic property [17]. On the other hand, Zhang et al. [18] observed RT FM in Fe- and Cu-codoped ZnO polycrystalline samples prepared

using the hydrothermal route; they found that Cu-doped ZnO:Fe leads to increase in magnetization. In contrast, Liu et al. [19] studied (Cu, Fe)-codoped ZnO powders synthesized using the sol–gel method, and they found that Cu doping greatly reduced the saturation magnetization (M_s). However, Jayakumar et al. studied Cu (1%)-doped $Zn_{0.95}Fe_{0.05}O$ nanocrystallites synthesized by a wet chemical route, and they attributed the observed RT FM in $Zn_{0.94}Fe_{0.05}Cu_{0.01}O$ to the formation of a secondary phase of Cu-doped $ZnFe_2O_4$ [20]. Also, Shim et al. [21] reported ferromagnetic behaviors for Fe-doped ZnO:Cu, FM was attributed to the $ZnFe_2O_4$ secondary phase. Thus, there are many controversies about the issue of the magnetic ground state in DMS systems. The ground state of DMS has been found to be very dependent on the synthesis method that is used. Consequently, the results of studies that have examined the effect of Cu or Mn on the magnetic properties of the Fe-doped ZnO DMS are still being disputed from both a theoretical and an experimental point of view.

Moreover, FM has been observed in undoped oxides, particularly in HfO_2 [22] and recently in ZnO [23–28]. Related calculations have demonstrated that defects in oxides, such as ZnO, TiO_2, HfO_2, and In_2O_3, can produce ferromagnetic behavior even without any doping [3]. However, the experimental results are very contradictory, and a basic understanding ferromagnetic behavior is still missing. Although oxygen defects are also broadly recognized as a possible reason for the ferromagnetic behavior of pure and doped ZnO, Sundaresan et al. [25] suggested oxygen defects ithemselves, and not TM ions, as the intrinsic origin of FM.

To explore the nature of the ferromagnetic ordering in 3d TM-doped oxide semiconductors, we study Fe-doped and (Cu/Mn, Fe)-codoped ZnO nanocrystalline samples in this paper. The present study attempted to synthesize a Fe-doped ZnO-based DMS samples by codoping Cu/Mn with Fe in ZnO. $Zn_{0.98-x}Fe_{0.02}(Cu/Mn)_xO$ ($x = 0.0$ and 0.02) nanoscale powders were synthesized using a solid-state reaction method. This technique offers several advantages such as low cost, easy controlling of the dopant amounts, facilitating production of bulk materials, and can avoid the chemical processes of fabrication as well as the influences of the substrate or the interface between the film and the substrate. Because of the low solubility of Fe in ZnO and a phase separation, and easy-to-form clusters or a

secondary phase of $ZnFe_2O_4$ for a dopant concentration >2 at.%, which suppressed the ferromagnetic ordering in the system [29], the Fe doping concentration of present investigation is limited to 2%. As for Cu codoping, the copper and corresponding oxides are nonmagnetic [30], so they cannot be a source for the increased ferromagnetic ordering in the ZnFeCuO samples. Therefore, codoping with Cu is considered as an ideal candidate to study the mechanism of FM in the ZnO-based DMS systems. On the other hand, since Mn is accepted as a contributor of higher individual magnetic moment of 4.93 μ_B [31], codoping with Mn would be an equally interesting issue to be addressed. However, our experimental results showed a very strong predominance of FM at RT in the Fe-doped ZnO samples, and codoping with Cu^{2+} or Mn^{2+} ions enhanced the M_s. The M_s value of the (Mn, Fe)-codoped ZnO is larger than that of the (Cu, Fe)-codoped ZnO, indicating the stronger ferromagnetic interactions in the (Mn, Fe)-codoped ZnO. The M_s value of the (Mn, Fe)-codoped ZnO is about one and a half times larger than that of the Fe-doped ZnO, and it is seven times larger than that of the undoped ZnO. However, the M_s of the Cu and Fe codoped ZnO is about five times larger than that of the undoped ZnO. On the other hand, the coercive field (H_c) values are 1295, 1220, and 785 G, for the ZnFeO, ZnFeCuO, and ZnFeMnO samples, respectively. The high coercivity fields obtained seem to result in a potential candidate to applications. The observed FM is interpreted based on the bound magnetic polarons (BMPs) model where the ferromagnetic ordering arises from indirect interaction between localized electrons of TM (3d) ions mediated by defects like oxygen vacancy in ZnO-based DMS system [3, 32]. Hence, in the codoped sample, the ferromagnetic coupling between TM–TM, Fe–Fe, and TM–Fe is mediated via clusters of V_O to favor the exchange interaction between the transitional metal ions which helps to have the long-range ferromagnetic ordering at RT. With the help of photoluminescence (PL) results, we have illustrated that V_O^+ (singly charged oxygen vacancies) is the key element for the RT FM in our samples. The presence of the very high oxygen vacancy concentration in the sample gives rise to the ferromagnetic ordering. This study of Cu or Mn/ZnO:Fe nanoscale powders is expected to contribute to a better understanding of ferromagnetic behavior in TM-doped ZnO materials.

However, it is of particular importance, to study the ferromagnetic properties in nanocrystalline materials as they will be potentially useful for ferrofluids, magnetic recording, and biomedical applications. The high saturation magnetizations of these systems imply that it can be used as magnetic nanostructure and possible future applications in permanent magnetism, magnetic recording, and spintronics.

Experimental details

The $Zn_{0.98-x}Fe_{0.02}(Cu/Mn)_xO$ ($x = 0.00$ and 0.02) nanopowders were synthesized using a solid-state reaction method from a stoichiometric mixture of ZnO (99.9% purity, Sigma-Aldrich), Fe_2O_3 (99.995%, Strem Chemicals, Inc.), Cu_2O (99.9%, Strem Chemicals, Inc.), and MnO_2 (99.995%, Strem Chemicals, Inc.). The mixture was first thoroughly mixed according to the desired stoichiometry, and then it was pre-fired at 400 °C for 8 h in air. The prepared powders were ground, pelletized, and annealed at 500 °C for 12 h in air to obtain nominal $Zn_{0.98-x}Fe_{0.02}$ $(Cu/Mn)_xO$ ($x = 0.00$ and 0.02) nanopowders. Undoped ZnO samples were also prepared under the same conditions. The crystalline structure of the samples was characterized by X-ray diffraction (XRD) (PANalytical X'Pert PRO). The optical absorption was measured using a CARY 5000 ultraviolet–visible (UV–vis) spectrophotometer with a wavelength ranging from 200 to 800 nm. The RT–PL spectra were measured in the range of 400–800 nm using a luminescence spectrometer (CARY Eclipse) at 381 nm. The magnetic properties of the samples were examined using a Lakeshore vibrating sample magnetometer (VSM) (model no. 7410).

Results and discussion

Figure 1 depicts the powder XRD patterns for the undoped ZnO, $Zn_{0.98}Fe_{0.02}O$ (ZFO), $Zn_{0.96}Fe_{0.02}Cu_{0.02}O$ (ZFCO), and $Zn_{0.96}Fe_{0.02}Mn_{0.02}O$ (ZFMO) nanopowders. The undoped sample shows the formation of hexagonal-ZnO (wurtzite structure type: space group $P6_{3mc}$) with Miller indices ($h\ k\ l$), as indicated on the diffraction peaks (Fig. 1). In addition to hexagonal-ZnO, a minuscule peak at ∼33° in the doped and codoped samples evolves as an additional plane of the α-Fe_2O_3 impurity phase (Fig. 1), which is consistent with earlier observations that the solubility
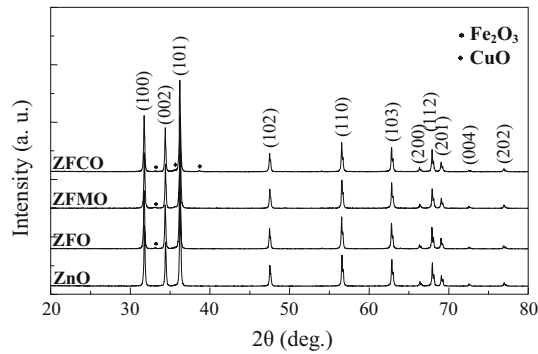
Figure 1 RT XRD patterns for ZnO, ZFO, ZFCO, and ZFMO.

of Fe in the ZnO crystal lattice is less than 2% [5] or less than 1% [33]. However, the XRD lines for the ZFCO sample also show two lines (a minuscule peak) of the CuO impurity phase, one at 35.63° and the other at 38.67°, along with hexagonal-ZnO [19]. This finding is consistent with the fact that the Cu solubility limit in ZnO is considerably low at ∼1% [4]. The diffraction peaks for the doped, and codoped samples slightly shift toward the lower angles, in comparison to ZnO. The 2θ degrees of the ZnO(002) diffraction peak are 34.452°, 34.404°, 34.412°, and 34.426° for the ZnO, ZFO, ZFCO, and ZFMO samples, respectively. This shift clearly suggests the incorporation of TMs into the ZnO lattice without altering the crystal structure. Calculation of the unit cell lattice parameters revealed that the shift is caused by the variation of the lattice parameters, a and c, which shows a small increase in comparison to ZnO. The cell parameters calculated for the undoped ZnO are $a = 3.2495$ Å and $c = 5.2065$ Å. The lattice parameters, a and c, and the unit cell volume (V) obtained from the XRD patterns are shown in Table 1. This increase was due to TM doping in ZnO, thus suggesting that the TM ions were incorporated into the lattice of the hexagonal wurtzite structure phase of ZnO [5, 18, 19, 34]. Because Fe^{2+} has a larger radius than Zn^{2+}, the cell size of ZFO would increase as the
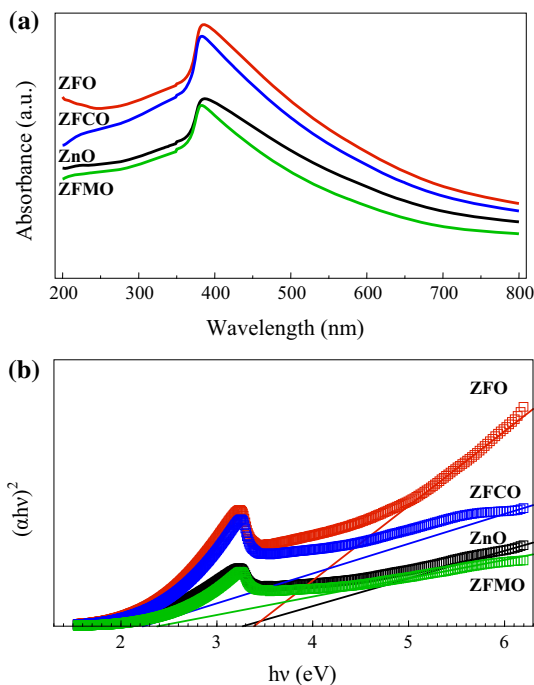
Fe dopants replace the Zn position in the ZFO lattice. This results in the following lattice parameters: $a = 3.2544$ Å and $c = 5.2090$ Å. The slight increase in the cell volume in the Cu-codoped case in comparison to the Mn-codoped case is inconsistent with the smaller ionic radius of Cu versus Mn. This may be due to the presence of more V_O in the ZFCO sample [32, 35], as demonstrated by the PL results (discussed below). This increase can also be explained by the segregation of small Cu ions and the formation of the CuO secondary phase [19] in the ZFCO sample (Fig. 1). This behavior is expected based on the difference between the ionic radii r of the tetrahedrally coordinated Zn^{2+} $r = 0.60$ Å and other TM^{2+} ions ($r = 0.66$, 0.63 and 0.57 Å for TM = Mn, Fe, and Cu, respectively). It is worth mentioning that in a stoichiometric wurtzite structure, the c/a ratio is 1.633. Our undoped and doped samples showed a significantly smaller c/a ratio (1.603 ± 0.001), and this might indicate the presence of V_O and extended defects [6]. From the XRD results, the degradation of XRD intensity was also observed with the incorporation of TM ions in the ZnO lattice (Fig. 1). The incorporation of 3d transition ions deteriorates the crystallinity of ZnO, due to their low solubility limit and various valence states [36]. The reduction in diffraction peak intensity and the increase in the full-width-at-half-maximum (FWHM) with the incorporation of TM ions, suggests the nanocrystalline nature of the samples. The average crystallite size for all the doped samples, which was determined from the broadening FWHM of the ZnO peaks of the XRD patterns using the Scherer formula, was found to be of 25.7 ± 0.35 nm; in comparison the average crystallite size for ZnO was 27.47 nm (Table 1). The marginal change in the average crystallite size due to doping and codoping confirms that any variation in the properties of the $Zn_{0.98-x}Fe_{0.02}(Cu/Mn)_xO$ ($x = 0.0$ and 0.02) samples with different TM ions are not due to any differences in the crystallite sizes.

Table 1 Lattice and magnetization parameters, and grain sizes for undoped ZnO, ZFO, ZFCO, and ZFMO nanopowders

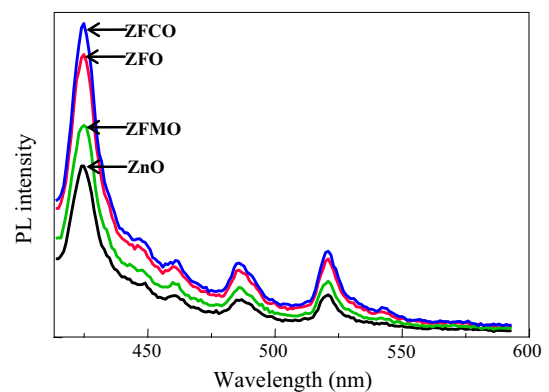| Samples	Lattice		Grain size (nm)	M_s (10^{-3} emu g^{-1})	M_{rs} (10^{-3} emu g^{-1})	H_c (G)
	Parameter (Å)	Volume (Å^3)				
ZnO	$a = 3.2495$, $c = 5.2065$	47.60	27.47	5.52	0.14	258
ZFO	$a = 3.2544$, $c = 5.2090$	47.76	26.05	26.45	3.13	1295
ZFCO	$a = 3.2532$, $c = 5.2120$	47.76	25.35	27.93	3.10	1220
ZFMO	$a = 3.2500$, $c = 5.2069$	47.62	25.89	39.07	2.84	785

The UV–Vis absorption spectra can further confirm evidence for TM substitution in the ZnO lattice. Figure 2a shows the UV–Vis absorption spectra of the ZnO, ZFO, ZFCO, and ZFMO nanopowders recorded at RT. The change in the absorption peak due to doping indicates a change in the band structure. In comparison with ZnO, the bandgap of the Fe-doped sample is shifted to higher energy [9, 33]. Based on the Burstein–Moss effect, the increase in the concentration of V_O broadens the optical bandgap and leads to the blueshift of the absorption spectra for oxide semiconductors. A redshift is also observed in the bandgap energy for both the Cu- or Mn-doped $Zn_{0.98}Fe_{0.02}O$ samples as compared to both the undoped and the Fe-doped ZnO samples. The redshift can be interpreted as mainly being the result of the sp–d exchange interactions between the ZnO band electrons and the localized "d" electrons associated with the doped TM^{2+} cations. The bandgaps of all of the samples was estimated through extrapolation of the linear portion of the $(\alpha h v)^2$ versus $h v$ curves, as shown in Fig. 2b. The calculated bandgaps of the ZnO, ZFO, ZFCO, and ZFMO samples are 3.27, 3.39, 2.23, and 2.38 eV, respectively. The ZFCO sample has the smallest bandgap compared to ZnO, ZFO,

and ZFMO, and this is due to the influence of the Cu content because CuO has a smaller bandgap of ~1.2 eV [37]. Kamarulzaman et al. [38] also obtained a small bandgap of 2.44 eV for Mn-doped ZnO nanostructure, while Thanh et al. [39] reported a decrease of bandgap from 3.15 to 1.28 eV for Mn-doped $SrTiO_3$ materials prepared by a solid-state reaction method when Mn increases from 0 to 10%. The change of bandgap with the composition indicates that the TM cations have been successfully incorporated into the ZnO crystal lattice, verifying that the observed RT FM (discussed below) is from TM substitution, not impurities.

Figure 3 illustrates the RT–PL measurements of all the samples. At RT, the PL spectra of the ZnO, ZFO, ZFCO, and ZFMO nanopowders (Fig. 3) show Vis emissions with five peaks, which are located at about 424 nm (violet emission), 448 and 461 nm (blue emission), and 486 and 521 nm (green emission). Obviously, the PL peaks shown in Fig. 3 are clearly due to ZnO, as they are also observed in the ZnO sample with no signal of TM-linked emission peaks. We have only noticed variations in the intensity of the PL peaks with different TMs. The shape of the PL spectra for the ZnO nanopowders is similar to those reported by others [23]. Commonly reported defects that are present in ZnO-based nanostructures are V_O with different charged states (V_O^x, V_O^+, V_O^{++} defect centers), zinc vacancies (V_{Zn}), a zinc interstitial (Zn_i) and an oxygen interstitial (O_i). V_{Zn} and O_i point defects may be thermodynamically established in the ZnO crystal lattice, but at a higher oxygen partial pressure [40]. Meanwhile, a Zn_i point defect has been demonstrated experimentally to be a very unstable defect [41]. Moreover, Zn_i is more likely to be annealed out at 400 °C than V_O, as shown by Herng

Figure 2 **a** RT UV–Vis absorption spectra of ZnO, ZFO, ZFCO, and ZFMO, and **b** $(\alpha h v)^2$ versus $h v$ values of ZnO, ZFO, ZFCO, and ZFMO.

Figure 3 RT–PL spectra of ZnO, ZFO, ZFCO, and ZFMO.
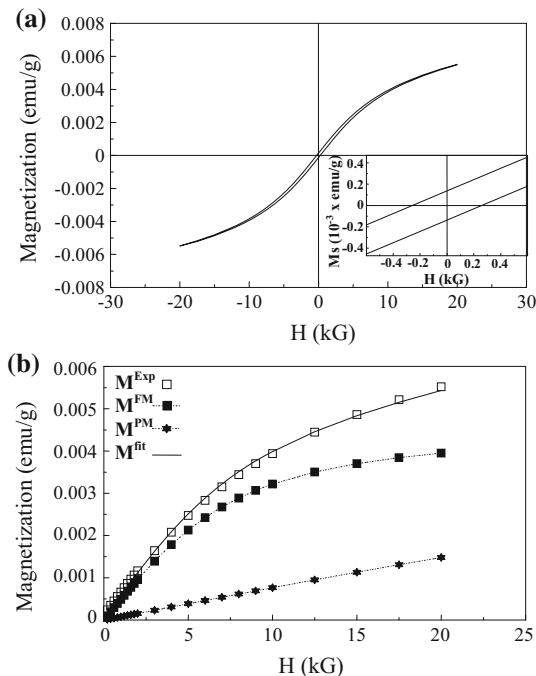
Figure 4 **a** RT *M*–*H* curve for ZnO. *Inset* shows RT hysteresis loop in a narrower field scale. **b** The initial portion of the *M*–*H* curve for ZnO—decomposition of the total measured magnetization (*M*) curve into its M^{FM} and M^{PM} components. The *solid line* represents the fit by the Langevin function.

et al. [42]. Note that, in our study, all of the samples were annealed in ambient air, resulting in an oxygen-deficient ZnO crystal [32, 35, 43, 44]; consequently, the Vis emission was most likely connected to the V_O defect. In comparison with ZnO, the intensity of the emission peaks was found to be enhanced for ZFO [9], and it decreased for ZFMO because Mn^{2+} dopants operate as a minimizer for the Vis luminescence of ZnO due to the formation of a large number of nonradiative centers on Mn doping [45, 46]. The intensity increased again for ZFCO, which was found to have the highest intensity [47].

However, the violet emission at 424 nm (2.92 eV) is almost certainly due to the electronic transition from the defect level (mainly V_O) presented at the grain boundaries and valence band [9, 24, 48]. Jin et al. [49] reported a similar explanation for ZnO prepared in an oxygen-deficient condition, with violet emission at 419 nm (2.95 eV). The XRD results in the present study (Fig. 1) indicate that the samples are nanocrystalline with increased surface-to-volume ratio, which leads to the largest increase in the concentration of defects (i.e., having a considerable

number of imperfections on their surfaces). This suggests that the oxygen-deficient phase was formed at the boundary between the nanoparticles. Moreover, V_O can be more easily formed, mainly on the surface or at the grain boundaries, due to the defective alignment of atoms [50]. Therefore, the samples may have more grain boundary defects that emit the violet luminescence with a higher intensity because they have smaller grains and a larger grain boundary area. Furthermore, it has been reported that interfacial traps, which are the V_O located within the depletion regions at the ZnO–ZnO grain boundaries, were about 0.33 eV below the conduction band edge [51]. As the ZnO bandgap energy was found to be 3.27 eV, the violet emission at 424 nm (2.92 eV) may be considered to be due to the near-band edge emission of the wide-bandgap ZnO, namely, the recombination of the free excitations. As for the blue peaks centered at 448 nm (2.77 eV) and 461 nm (2.69 eV), neutral oxygen vacancies (V_O^x) are also regarded as luminescent centers. V_O has been reported to be the origin of the ZnO blue emission [23, 52–54]. Wu et al. have previously reported the blue emission at $\sim$2.8 eV from ZnO nanowhiskers [48]. Furthermore, the V_O of ZnO has been predicted to be at $\sim E_V + 2.7$ eV [55] or $\sim E_V + 2.78$ eV [56], which is consistent with the photon energy of the blue emissions observed in this present study. Based on these reports, we suggest that the blue emissions of our samples may be caused by the electron transition from V_O^x centers to the valence band edge [48, 56]. This is also due to the oxygen-deficient phase at the boundary between the nanoparticles. In bulk ZnO, the V_O^x centers are not underactive ionized, which is a response to the absence of blue emission in bulk ZnO [56]. It is accepted that the green luminescence peaks centered at about 486 nm (2.55 eV) and 521 nm (2.38 eV) are due to V_O^+ [24, 26, 52, 53, 57]. The singly charged center (V_O^+) in the absence of a depletion region becomes the neutral center (V_O^x) through the capture of an electron from the conduction band, which then recombines with a hole in the valence band, giving rise to emissions at 486 nm (2.55 eV) and 521 nm (2.38 eV) [52]. Grain boundaries and intrinsic defects, such as V_O, may also enhance FM as reported by Straumal et al. [27]. A singly occupied oxygen vacancy (oxygen vacancy with one electron; unpaired electrons) with a spin of 1/2 has been previously ascribed to the origin of RT FM in ZnO [25–27].
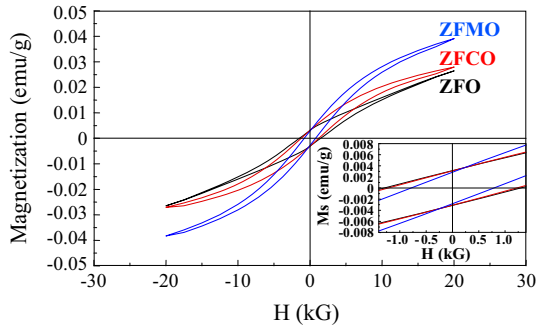
Figure 5 RT M–H curves for ZFO, ZFCO, and ZFMO. *Inset* shows the RT hysteresis loops in a narrower field scale.

We have investigated the magnetic properties of undoped ZnO and $Zn_{0.98-x}Fe_{0.02}(Cu/Mn)_xO$ ($x = 0.0$ and 0.02) nanopowders using VSM. The field-dependent magnetization (M–H) curve recorded for ZnO at RT is shown in Fig. 4a. The inset in the figure shows the RT hysteresis loop in a narrower field scale. As seen in the figure, the sample exhibits a clear hysteresis loop with an H_c of 258 Oe and an M_s of 5.52×10^{-3} emu g^{-1} [23] (Table 1 and the inset of Fig. 4a), revealing an RT FM characteristic. The observed M_s of 5.52×10^{-3} emu g^{-1} for ZnO is larger than the M_s values of 4.0×10^{-3} emu g^{-1} [26] and 0.784×10^{-3} emu g^{-1} [24] obtained for pure ZnO. Sundaresan et al. [25] also reported FM in pure ZnO nanoparticles, and they intend for FM to be the universal feature of the nanoparticles of nonmagnetic oxides. They also explained that the origin of FM in these nanoparticles is due to the location of V_O at the surface of nanoparticles, which is due to the loss of oxygen. It may be useful to point out that ZnO powders heated at a high temperature, even in the air, would lose oxygen [35, 43]. Therefore, the RT FM in our ZnO is due to V_O-induced spin polarization (induced d^0 FM). Thus, the unpaired electron that spins on the surface of the particles is responsible for FM in the ZnO nanopowders.

As seen in Fig. 4a, the curve shows a hysteretic feature coupled with a PM-like signal. Therefore, it seems reasonable to express the total magnetization of the sample as a sum of two components:

$$M(H) = M^{FM}(H) + M^{PM}(H), \qquad (1)$$

where M^{FM} is the contribution of FM and M^{PM} describes the contribution coming from the PM particles. We could successfully fit the field dependence of magnetization for the ZnO using the relation: $M(H) = M_s L(\mu H/k_B T) + \chi_P H$, where M_s is the

saturation magnetization, μ is the magnetic moment of an individual particle, $L(x) = \coth(x) - (1/x)$ is the well-known Langevin function, μ is a measure of the magnitude of the moment on a particle, k_B is the Boltzmann constant, and χ_P is the PM susceptibility. The entire fitting demagnetization curve is made by the superposition of both the FM and PM fitting functions. These curves, along with the experimental data for ZnO, are shown in Fig. 4b, and the agreement between theory and experiment is evident. The average moment per particle obtained from the fit is 1.4×10^3 μ_B, which is in agreement with that observed for Sn nanoparticles [58] and GaN nanoparticles [59]. From the average moment per particle, we have estimated the number of defects to be 2.6×10^{18} cm^{-3}, which is comparable to the finding reported by the Rao and colleagues [59].

Figure 5 shows the M–H at RT for ZFO, indicating ferromagnetic hysteresis. The RT M versus H data of ZFO showed a linear component superimposed on a saturating FM-like magnetization. The FM/PM behavior is due to the incorporation of Fe ions into the host lattice. If this linear component is subtracted, the M versus H data show saturation of the M expected for an ferromagnetic phase (Fig. 5). These results indicate that a fraction of the doped Fe is not participating in the ordered magnetic state and is present the PM state. The M_s value is ~ 0.026 emu g^{-1}, which exceeds the previously reported values for ZnO:Fe DMS materials [7, 9, 24], but it is smaller than the M_s observed for other iron doped ZnO DMS materials [8]. Still, the magnetization data shown in Fig. 5 clearly displays an open loop, and ZFO displays a H_c of 1295 Oe (Table 1 and the inset of Fig. 5). This value is similar to, or higher than, the H_c obtained for ZnO:Fe DMS system [7–9], but it is smaller than the H_c value (1984 Oe) observed for Fe-doped ZnO nanostructures prepared using a chemical route [34]. The presence of clear H_c rules out the possibility of superparamagnetism and supports a ferromagnetic origin [7]. Because the solid-state reaction method preparation of the samples, and their subsequent calcining and sintering processes, were all conducted in air, it intrinsically eliminated the metallic Fe particles. On the other hand, the maghemite (γ-Fe$_2$O$_3$) phase converted to the hematite (α-Fe$_2$O$_3$) phase when annealed at temperatures above 350 °C [60, 61]. Additionally, the hematite phase is thermally the most stable phase, and it undergoes a thermal reduction in the magnetite

(Fe$_3$O$_4$) phase only above 1200 °C [61]. By recalling the XRD data we discussed earlier, which clearly ruled out the possible presence of metallic Fe, one observes only the secondary α-Fe$_2$O$_3$ phase. Furthermore, the random presence of α-Fe$_2$O$_3$ impurities is unlikely to produce a similar magnetization with a high H_c value of 1295 Oe. H_c values in the range of 20–50 Oe have been reported for α-Fe$_2$O$_3$, γ-Fe$_2$O$_3$, Fe$_3$O$_4$, and ZnFe$_2$O$_4$ [8, 10]. For all of the above reasons, we believe that FM in our samples is an intrinsic property, and it is not due to the presence of iron-phase impurities.

ZnO:0.02Fe nanopowders codoped with other TM elements, such as Cu or Mn, were also investigated using VSM. The results show the presence of FM at RT. Unlike the remnant magnetization (M_r) or H_c [16], M_s increased with the samples that were codoped with Cu or Mn atoms. The M versus H curves for ZFCO and ZFMO are also shown in Fig. 5, after the removal of a linear response term from the raw data. For the ZFCO, the sample has a well-defined hysteresis at RT with a H_c of 1220 Oe and a M_r of 3.10 × 10^{-3} emu g^{-1} (Table 1 and the inset of Fig. 5). The corresponding values for the sample codoped with Mn are, respectively, 785 Oe and 2.84 × 10^{-3} emu g^{-1}. It is interesting to note that the M_s is higher for ZFO codoped with the Mn element compared with that codoped with Cu. The RT M_s is ∼0.028 emu g^{-1} for ZFCO and is ∼0.039 emu g^{-1} for ZFMO. Both M_s values are higher than the value of ∼0.026 emu g^{-1} observed for ZFO. The fact that M_s increases with codoped both with Cu or Mn atoms eliminates the possibility of Fe (or iron oxide) clusters' being responsible for magnetization. It appears that codoping with Mn considerably enhances M_s, while codoping with Cu might improve M_s to some extent; it seems mostly related to the presence of the CuO impurity phase [30] in ZFCO. The M_s value of the ZFMO is about one and a half times larger than that of the ZFO, and it is seven times larger than that of ZnO, while, the M_s value of the ZFCO is about five times larger than that of ZnO. These results clearly imply that the M_s values obtained in Zn$_{0.96}$Fe$_{0.02}$(Cu/Mn)$_{0.02}$O depend on the starting materials as well as the surface defects (V_O^+) in the metal–oxide host system [5], as the PL studies explain.

However, the possibility of the origination of FM in our ZFCO sample from the Cu-related secondary phases, including metallic Cu and its oxides (Cu$_2$O and CuO), may be excluded because they are generally considered to be nonferromagnetic [30]. Therefore, the FM of the ZFCO may be unrelated to the appearance of the CuO phase, and the FM observed in the sample is expected to be intrinsic. On the other hand, neither Mn metal nor any oxide of Mn is ferromagnetic except for Mn$_3$O$_4$, with a Curie temperature around 45 K. Therefore, the possibility of RT FM in ZFMO originated from segregated Mn or Mn-related oxides, is excluded [62]. We believe that the RT FM in Zn$_{0.98-x}$Fe$_{0.02}$(Cu/Mn)$_x$O ($x = 0.0$ and 0.02) nanopowders is intrinsic and it may be related to variations of the sample defect structure and/or V_O. However, it is evident from a wide variety of experimental results that point defects, that is V_O, are responsible for the ferromagnetic response present in the undoped and TM-doped ZnO samples [22, 25–27]. Our previous work also found that V_O are rather important to the observed FM in copper-doped ZnO [32]. The formation of V_O is clearly evident from the PL spectra of all the samples. From the above observations and the PL results, we suggest that singly charged V_O^+, located on the surface, with an unpaired electron, in addition to localized "**d**" spins on the TM ions, are responsible for the RT FM of undoped and TM-doped ZnO nanopowders. This correlation favors the formation of BMPs as the origin of RT FM [3]. Defects tend to form BMPs that couple with 3d moments within their orbits. The overlapping of magnetic polarons induces spin–spin interactions between magnetic ions, eventually stabilizing the ferromagnetic ordering.

Conclusions

We have synthesized Zn$_{0.98-x}$Fe$_{0.02}$(Cu/Mn)$_x$O ($x = 0.0$ and 0.02) nanopowders using a solid-state reaction method. UV–Vis measurements demonstrated that the bandgap increased in Fe-doped ZnO and decreased in both Cu- or Mn-doped Zn$_{0.98}$Fe$_{0.02}$O. PL studies confirmed the formation of oxygen vacancies (V_O) in all of the samples. The VSM measurement results showed an enhancement in the saturation magnetization (M_s) value due to codoping. The magnetization measurements demonstrate that doping with Fe alone can improve the M_s in ZnO, while codoping with Mn obviously enhances M_s, and codoping with Cu might increase M_s to some extent, but not as critically as theories have expected. The M_s

value of the Mn/ZnO:Fe is larger than that of the Cu/ZnO:Fe, indicating the stronger ferromagnetic interactions in Mn/ZnO:Fe. The M_s value of the Mn/ZnO:Fe is about one and a half times larger than that of the ZnO:Fe, and it is seven times larger than that of the undoped ZnO. However, the M_s of Cu/ZnO:Fe is about five times larger than that of the undoped ZnO. A detailed analysis based on the magnetic measurement rules out FM due to α-Fe$_2$O$_3$ and/or CuO impurities. Based on these experiments, we believe that the FM is intrinsic and is probably due to interactions between substitutional TM$_{Zn}$ and other (intrinsic) point defects, most likely V_O, in the crystal.

Compliance with ethical standards

Conflicts of interest   The author declares that he has no conflict of interest.

References

[1] Ohno H (1998) Making nonmagnetic semiconductors ferromagnetic. Science 281:951–956

[2] Dietl T, Ohno H, Matsukura F, Cibert J, Ferrand D (2000) Zener model description of ferromagnetism in zinc-blende magnetic semiconductors. Science 287:1019–1022

[3] Coey JMD, Venkatesan M, Fitzgerald CB (2005) Donor impurity band exchange in dilute ferromagnetic oxides. Nat Mater 4:173–179

[4] Park MS, Min BI (2003) Ferromagnetism in ZnO codoped with transition metals: Zn$_{1-x}$(FeCo)$_x$O and Zn$_{1-x}$(FeCu)$_x$O. Phys Rev B 68:224436–224441

[5] Chakrabarti M, Dechoudhury S, Sanyal D, Roy TK, Bhowmick D, Chakrabarti A (2008) Observation of room temperature ferromagnetism in Mn–Fe doped ZnO. J Phys D 41:135006-1–135006-5

[6] Beltrán JJ, Osorio JA, Barrero CA, Hanna CB, Punnoose A (2013) Magnetic properties of Fe doped, Co doped, and Fe + Co co-doped ZnO. J Appl Phys 113:17C308-1–17C308-3

[7] Johnson LM, Thurber AP, Anghel J, Sabetian M, Engelhard MH, Tenne DA, Hanna CB, Punnoose A (2010) Transition metal dopants essential for producing ferromagnetism in metal oxide nanoparticles. Phys Rev B 82:054419-1–054419-5

[8] Wang F, Huang W-W, Li S-Y, Lian A-Q, Zhang X-T, Cao W (2013) The magnetic properties of Fe$_x$Zn$_{1-x}$O synthesized via the solid-state reaction route: experiment and theory. J Magn Magn Mater 340:5–9

[9] Kumar S, Mukherjee S, Singh RKr, Chatterjee S, Ghosh AK (2011) Structural and optical properties of sol-gel derived nanocrystalline Fe-doped ZnO. J Appl Phys 110:103508-1–103508-7

[10] Jayakumar OD, Gopalakrishnan IK, Vinu A, Asthana A, Tyagi AK (2008) Room temperature ferromagnetism in Th$_{1-x}$Fe$_x$O$_{2-\delta}$ (x = 0.0, 0.05, 0.10, 0.15, 0.20 and 0.25) nanoparticles. J Alloys Compd 461:608–611

[11] Yang HL, Xu XG, Wu SZ, Wu K, Ai C, Miao J, Jiang Y (2012) Effects of dopants on magnetic properties of Cu-doped ZnO thin films. J Mater Sci 47:530–533. doi:10.1007/s10853-011-5830-z

[12] Krishnamoorthy S, Iliadis AA (2006) Development of high frequency love mode surface acoustic wave ZnO/SiO$_2$/Si devices. Solid State Electron 50:1113–1118

[13] Sharma PK, Dutta PK, Pandey AC, Layek S, Verma HC (2009) Effect of iron doping concentration on magnetic properties of ZnO nanoparticles. J Magn Mater 321:2587–2591

[14] Han S-J, Song JW, Yang C-H, Park SH, Park J-H, Jeong YH, Rhie KW (2002) A key to room-temperature ferromagnetism in Fe-doped ZnO:Cu. Appl Phys Lett 81:4212–4213

[15] Aljawfi RN, Mollah S (2011) Properties of Co/Ni codoped ZnO based nanocrystalline DMS. J Magn Magn Mater 323:3126–3132

[16] Mandal SK, Nath TK, Das A (2007) Reduction of magnetization in Zn$_{0.9}$Fe$_{0.1}$O diluted magnetic semiconducting nanoparticles by doping of Co or Mn ions. J Appl Phys 101:123920-1–123920-7

[17] Fan JP, Jiang FX, Quan ZY, Qing XF, Xu XH (2012) Different magnetic origins of (Mn, Fe)-codoped ZnO powders and thin films. Mater Res Bull 47:3344–3347

[18] Zhang H-W, Wei Z-R, Li Z-Q, Dong G-Y (2007) Room-temperature ferromagnetism in Fe-doped, Fe- and Cu-codoped ZnO diluted magnetic semiconductor. Mater Lett 61:3605–3607

[19] Liu HL, Yang JH, Hua Z, Liu Y, Yang LL, Zhang YJ, Cao J (2011) Cu-doping effect on structure and magnetic properties of Fe-doped ZnO powders. Mater Chem Phys 125:656–659

[20] Jayakumar OD, Gopalakrishnan IK, Kulshreshtha SK (2006) Magnetization study of Fe-doped ZnO co-doped with Cu: synthesized by wet chemical method. J Mater Sci 41:4706–4712. doi:10.1007/s10853-006-0045-4

[21] Shim JH, Hwang T, Lee S, Park JH, Han SJ, Jeong YH (2005) Origin of ferromagnetism in Fe- and Cu-codoped ZnO. Appl Phys Lett 86:082503-1–082503-3

[22] Venkatesan M, Fitzgerald CB, Coey JMD (2004) Thin films: unexpected magnetism in a dielectric oxide. Nature 430:630

[23] Mary JA, Vijaya JJ, Dai JH, Bououdina M, Kennedy LJ, Song Y (2015) Experimental and first-principles DFT studies of electronic, optical and magnetic properties of cerium–manganese codoped zinc oxide nanostructures. Mater Sci Semicond Process 34:27–38

[24] Fabbiyola S, Kennedy LJ, Ratnaji T, Vijaya JJ, Aruldoss U, Bououdina M (2016) Effect of Fe-doping on the structural, optical and magnetic properties of ZnO nanostructures synthesized by co-precipitation method. Ceram Int 42: 1588–1596

[25] Sundaresan A, Bhargavi R, Rangarajan N, Siddesh U, Rao CNR (2006) Ferromagnetism as a universal feature of nanoparticles of the otherwise nonmagnetic oxides. Phys Rev B 74:161306(R)

[26] Yılmaz S, Garry S, McGlynn E, Bacaksız E (2014) Synthesis and characterization of Mn-doped ZnO nanorods grown in an ordered periodic honeycomb pattern using nanosphere lithography. Ceram Int 40:7753–7759

[27] Straumal BB, Mazilkin AA, Protasova SG, Myatiev AA, Straumal PB, Schütz G, van Aken PA, Goering E, Baretzky B (2009) Magnetization study of nanograined pure and Mn-doped ZnO films: formation of a ferromagnetic grain-boundary foam. Phys Rev B 79:205206-1–205206-6

[28] Golmar F, Villafuerte M, Navarro AM, Torres CER, Barzola-Quiquia J, Esquinazi P, Heluani SP (2010) ZnO:Co diluted magnetic semiconductor or hybrid nanostructure for spintronics? J Mater Sci 45:6174–6178. doi:10.1007/s10853-010-4710-2

[29] Wang YQ, Yuan SL, Liu L, Li P, Lan XX, Tian ZM, He JH, Yin SY (2008) Ferromagnetism in Fe-doped ZnO bulk samples. J Magn Magn Mater 320:1423–1426

[30] Brumage WH, Dorman CF, Quade CR (2001) Temperature-dependent paramagnetic susceptibilities of Cu^{2+} and Co^{2+} as dilute impurities in ZnO. Phys Rev B 63:104411-1–104411-4

[31] Yun SY, Cha G-B, Kwon YS, Cho S, Hong SC (2004) First-principles calculations on magnetism of transition metal doped zinc oxide. J Magn Magn Mater 272(276):e1563–e1564

[32] Ahmed SA (2016) Effects of annealing temperature and dopant concentration on the structure, optical, and magnetic properties of Cu-doped ZnO nanopowders. J Mater Sci Mater Electron. doi:10.1007/s10854-016-5981-4

[33] Sahai A, Kumar Y, Agarwal V, Olive-Méndez SF, Goswami N (2014) Doping concentration driven morphological evolution of Fe doped ZnO nanostructures. J Appl Phys 116:164315-1–164315-12

[34] Mishra AK, Das D (2010) Investigation on Fe-doped ZnO nanostructures prepared by a chemical route. Mater Sci Eng B 171:5–10

[35] Dutta S, Chakrabarti M, Chattopadhyay S, Jana D, Sanyal D, Sarkar A (2005) Defect dynamics in annealed ZnO by positron annihilation spectroscopy. J Appl Phys 98:53513-1–53513-5

[36] Jimenez-Gonzalez AE (1997) Modification of ZnO thin films by Ni, Cu, and Cd doping. J Solid State Chem 128:176–180

[37] Johan MR, Suan MSM, Hawari NL, Ching HA (2011) Annealing effects on the properties of copper oxide thin films prepared by chemical deposition. Int J Electrochem Sci 6:6094–6104

[38] Kamarulzaman N, Kasim MF, Rusdi R (2015) Band gap narrowing and widening of ZnO nanostructures and doped materials. Nanoscale Res Lett 10:346

[39] Thanh TD, Phan TL, Oanh LM, Minh NV, Lee JS, Yu SC (2014) Influence of Mn doping on the crystal structure, and optical and magnetic properties of $SrTiO_3$ compounds. IEEE Trans Magn 50:2502704-1–2502704-4

[40] Tuomisto F, Ranki V, Saarinen K, Look DC (2003) Evidence of the Zn vacancy acting as the dominant acceptor in n-type ZnO. Phys Rev Lett 91:205502-1–205502-4

[41] Vlasenko LS, Watkins GD (2005) Optical detection of electron paramagnetic resonance for intrinsic defects produced in ZnO by 2.5-MeV electron irradiation in situ at 4.2 K. Phys Rev B 72:035203-1–035203-12

[42] Herng TS, Lau SP, Yu SF, Yang HY, Wang L, Tanemura M, Chen JS (2007) Magnetic anisotropy in the ferromagnetic Cu-doped ZnO nanoneedles. Appl Phys Lett 90:032509-1–032509-3

[43] Sanyal D, Roy TK, Chakrabarti M, Dechoudhury S, Bhowmick D, Chakrabarti A (2008) Defect studies in annealed ZnO by positron annihilation spectroscopy. J Phys Condens Matter 20:45217-1–45217-4

[44] Mishra AK, Chaudhuri SK, Mukherjee S, Priyam A, Saha A, Das D (2007) Characterization of defects in ZnO nanocrystals: photoluminescence and positron annihilation spectroscopic studies. J Appl Phys 102:103514-1–103514-6

[45] Philipose U, Nair SV, Trudel S, de Souza CF, Aouba S, Hill RH, Ruda HE (2006) High-temperature ferromagnetism in Mn-doped ZnO nanowires. Appl Phys Lett 88:263101-1–263101-3

[46] Chen L-C, Tien C-H, Fu C-S (2012) Magneto-optical characteristics of Mn-doped ZnO films deposited by ultrasonic spray pyrolysis. Mater Sci Semicond Process 15:80–85

[47] Sharma PK, Kumar M, Pandey AC (2011) Green luminescent $ZnO:Cu^{2+}$ nanoparticles for their applications in white-light generation from UV LEDs. J Nanopart Res 13:1629–1637

[48] Wu R, Yang Y, Cong S, Wu Z, Xie C, Usui H, Kawaguchi K, Koshizaki N (2005) Fractal dimension and photoluminescence of ZnO tetrapod nanowhiskers. Chem Phys Lett 406:457–461

[49] Jin BJ, Im S, Lee SY (2000) Violet and UV luminescence emitted from ZnO thin films grown on sapphire by pulsed laser deposition. Thin Solid Films 366:107–110

[50] Liu XJ, Zhu XY, Luo JT, Zeng F, Pan F (2009) Grain boundary defects-mediated room temperature ferromagnetism in Co-doped ZnO film. J Alloys Compd 482:224–228

[51] Cordaro JF, Shim Y, May JE (1986) Bulk electron traps in zinc oxide varistors. J Appl Phys 60:4186–4190

[52] Ghosh M, Raychaudhuri AK (2008) Shape transition in ZnO nanostructures and its effect on blue-green photoluminescence. Nanotechnology 19:445704-1–445704-7

[53] Monticone S, Tufeu R, Kanaev AV (1998) Complex nature of the UV and visible fluorescence of colloidal ZnO nanoparticles. J Phys Chem B 102:2854–2862

[54] Kim JH, Yu JH, Kim TS, Jeong TS, Youn CJ, Hong KJ (2010) Electric-field effect of near-band-edge photoluminescence in bulk ZnO. J Mater Sci 45:4036–4039. doi:10.1007/s10853-010-4483-7

[55] Van de Walle CG (2001) Defect analysis and engineering in ZnO. Physica B 308–310:899–903

[56] Liao Z-M, Zhang H-Z, Zhou Y-B, Xu J, Zhang J-M, Yu D-P (2008) Surface effects on photoluminescence of single ZnO nanowires. Phys Lett A 372:4505–4509

[57] Mesaros A, Toloman D, Nasui M, Mos RB, Petrisor T, Vasile BS, Surdu VA, Perhaita I, Biris A, Pana O (2015) A valence states approach for luminescence enhancement by low dopant concentration in Eu-doped ZnO nanoparticles. J Mater Sci 50:6075–6086. doi:10.1007/s10853-015-9157-z

[58] Li W-H, Wang C-W, Li C-Y, Hsu CK, Yang CC, Wu C-M (2008) Coexistence of ferromagnetism and superconductivity in Sn nanoparticles. Phys Rev B 77:094508-1–094508-7

[59] Madhu C, Sundaresan A, Rao CNR (2008) Room-temperature ferromagnetism in undoped GaN and CdS semiconductor nanoparticles. Phys Rev B 77:201306-1–201306-4

[60] Punnoose A, Hays J, Thurber A, Engelhard MH, Kukkadapu RK, Wang C, Shutthanandan V, Thevuthasan S (2005) Development of high-temperature ferromagnetism in SnO_2 and paramagnetism in SnO by Fe doping. Phys Rev B 72:054402-1–054402-14

[61] Zboril R, Mashlan M, Petridis D (2002) Iron(III) oxides from thermal processes synthesis, structural and magnetic properties, Mössbauer spectroscopy characterization, and applications. Chem Mater 14:969–982

[62] Ahmed SA (2009) Structure and magnetism of manganese-doped ZnO powder samples. Cryst Res Technol 44:971–977